Insights into Water Mass Origins in the Central Arctic Ocean from in-situ Dissolved Organic Matter Fluorescence.

Colin A. Stedmon[1*]; Rainer M.W. Amon[2,3], Dorothea Bauch[4,5] Astrid Bracher[6,7,] Rafael Gonçalves-Araujo[1]; Mario Hoppmann[6]; Richard Krishfield[8]; Samuel Laney[8]; Benjamin Rabe[6]; Heather Reader[9]; Mats A. Granskog[10]

[1] National Institute for Aquatic Resources, Technical University of Denmark, Lyngby, Denmark.

[2] Texas A&M University, Department of Marine and Coastal Environmental Science, Galveston, USA

[3] Texas A&M University, Department of Oceanography, College Station, USA

[4] Leibniz Laboratory, University of Kiel, Kiel, Germany

[5] GEOMAR Helmholtz Centre for Ocean Research Kiel, Kiel, Germany

[6] Alfred-Wegener-Institut Helmholtz-Zentrum für Polar- und Meeresforschung, Bremerhaven, Germany

[7] Institute of Environmental Physics, Faculty of Physics and Electrical Engineering, University Bremen, Bremen, Germany

[8] Woods Hole Oceanographic Institution, Woods Hole, Massachusetts, USA.

[9] Department of Chemistry, Memorial University of Newfoundland, St John's, Canada.

[10] Norwegian Polar Institute, Fram Centre, Tromsø, Norway.

Corresponding author: Colin A. Stedmon (cost@aqua.dtu.dk)

Key Points:

- Arctic surface waters with comparable temperature and salinity have contrasting in situ dissolved organic matter fluorescence.
- Organic matter fluorescence can track low salinity waters feeding into the Transpolar Drift and halocline layers.
- Siberian and Chukchi shelf waters can be separated based on their fluorescence to salinity relationship.

Abstract

The Arctic Ocean receives a large supply of dissolved organic matter (DOM) from its catchment and shelf sediments, which can be traced across much of the basin's upper waters. This signature can potentially be used as a tracer. On the shelf, the combination of river discharge and sea-ice formation, modifies water densities and mixing considerably. These waters are a source of the halocline layer that covers much of the Arctic Ocean, but also contain elevated levels of DOM. Here we demonstrate how this can be used as a supplementary tracer and contribute to evaluating ocean circulation in the Arctic. A fraction of the organic compounds that DOM consists of fluoresce and can be measured using in-situ fluorometers. When deployed on autonomous platforms these provide high temporal and spatial resolution measurements over long periods. The results of an analysis of data derived from several Ice Tethered Profilers (ITPs) offer a unique spatial coverage of the distribution of DOM in the surface 800m below Arctic sea-ice. Water mass analysis using temperature, salinity and DOM fluorescence, can clearly distinguish between the contribution of Siberian terrestrial DOM and marine DOM from the Chukchi shelf to the waters of the halocline. The findings offer a new approach to trace the distribution of Pacific waters and its export from the Arctic Ocean. Our results indicate the potential to extend the approach to separate freshwater contributions from, sea-ice melt, riverine discharge and the Pacific Ocean.

1 Introduction

The central Arctic Ocean is surrounded by expansive shelf seas which influence ocean circulation and seawater properties (Figure 1). Shallow depths restrict deep water exchange to only occur in the Fram Strait. Much of the surface water inflow occurs over the expansive shelf sea areas, where river runoff and extensive seasonal sea-ice formation and melt modify the physical and chemical properties. Inflowing waters from the Pacific and Atlantic also loose heat to the atmosphere and are cooled during their passage over the shelves (Dmitrenko et al., 2009; Rudels et al., 1996; Rudels et al., 2000; Shimada, 2005). These waters are gradually modified and diluted by the freshwater discharge from major rivers with catchments in North America and Eurasia (Haine et al., 2015; Overeem & Syvitski, 2010; Peterson et al., 2002; Serreze et al., 2006). Sea-ice formation and subsequent export of ice off the shelf partially counteracts this dilution (Bauch et al., 2009, 2011). Brine rejection results in the formation of shelf waters very close to freezing temperature and with slightly increased salinity, as well as other dissolved constituents (Anderson et al., 1988).

The chemical composition of inflowing oceanic water is also altered during its passage over the shelves. Rivers supply high concentrations of terrestrial dissolved organic matter (DOM) (Amon et al., 2012). While inorganic nutrient concentrations in Arctic rivers are comparable to oceanic concentrations (Holmes et al., 2012), dissolved organic carbon (DOC) concentrations are an order of magnitude higher than in inflowing ocean water (Anderson & Amon, 2015). Further, interactions with shelf sea sediments also influence the chemical composition of these waters, as degradation and dissolution of particulate organic matter results in high porewater concentrations of DOC which subsequently diffuse to overlying waters (Chen et al., 2016). Concentrations of nutrients in shelf bottom waters are also higher as a result of elevated rates of organic matter mineralization (Bauch et al., 2011; Dmitrenko et al., 2011; Jones & Anderson, 1986). Denitrification in organic rich sediments is a sink for nitrate and results in

shelf waters having a nitrogen deficit relative to phosphate, in comparison to sub-Arctic ocean waters (Anderson et al., 2013; Codispoti et al., 2005; Hardison et al., 2017; Jones & Anderson, 1986). Passage over the shelf therefore imparts a detectable chemical signature which is then entrained into the larger scale circulation of the Arctic basin.

Surface waters of the Arctic Ocean are often referred to as the Polar Mixed Layer (PML; e.g. Korhonen et al., 2013), which is shaped by repeated convective mixing due to brine release from seasonal ice formation. It is often re-stratified during the melting season, bounded at the bottom by a temperature minimum that is a remnant of the deeper mixed layer from the previous winter's convection (Korhonen et al., 2013; Peralta-Ferriz & Woodgate, 2015; Rudels et al., 2004). Below this, a striking characteristic of the water column in the Arctic Ocean is the widespread presence of a halocline layer (HL) (Coachman & Aagaard, 1974), which consists of cold waters with temperatures close to the freezing point for their given salinity, and salinities ranging between 28-34.8 (Korhonen et al., 2013). The HL is fed by brine rejection (associated with sea-ice formation) and convection occurring in open waters (Steele & Boyd, 1998) or in adjacent shelf seas and subsequently advected off-shore (Aagaard et al., 1981). Halocline waters can extend from near the surface (in areas of formation) to as deep as ~300 m in the southern Amerasian Basin. The HL separates surface waters from warmer waters of Atlantic origin below (hereafter referred to as Atlantic Water, AW). The stratification maintained by the halocline facilitates the formation and persistence of sea-ice in the Arctic as the PML is largely insulated from contact with warmer Atlantic waters below (Aagaard et al., 1981; Toole et al., 2010). Ice free waters of the greater Arctic region are as such due to the absence of a persistent cold halocline layer (Polyakov et al., 2020) or increased retention of summer heat in PML (Timmermans et al., 2018).

The HL in the Arctic Ocean differs in composition and structure depending on location. The lower halocline (LHC) has its origins in waters from the Atlantic and extends from a salinity of 34 to the depth of the 0 °C isotherm (Korhonen et al., 2013). It is formed near the inflow regions of AW north of the Fram Strait, the southern Nansen Basin and the Barents Sea (Rudels et al., 1996). This forms the main transition between the PML, which has properties that vary seasonally, and the deeper AW with potential temperatures above 0 ºC. In the Amerasian Basin the HL extends deeper and is composed by two distinct layers: the upper halocline (UHC), right underneath the PML (temperature minimum) and the LHC originating from the Eurasian Basin (Rudels et al., 2004). The UHC is composed of low salinity water from the Pacific inflow (S~32.5) (Coachman & Barnes, 1961) and a variable contribution from the East Siberian Sea (Anderson et al., 2017). This is subject to seasonal variability and lateral intrusion of Pacific or dense water formed during ice formation on the shelves (Bauch et al., 2014; Jones & Anderson, 1986). Contributions to the UHC are Pacific Summer Water (PSW) recognizable as a distinct temperature maximum (warmer than -1 °C) with salinities between 31 and 33 (Steele et al., 2004) and below this is a temperature minimum representing Pacific Winter Water (PWW) with salinities of about 33.1 (Coachman & Barnes, 1961). Above the Amerasian UHC a near surface temperature maximum (NSTM) can develop due to summertime warming from solar radiation which is subsequently covered by a shallow surface layer of fresh water from ice melt (Jackson et al., 2010).

Another distinct oceanographic feature in the central Arctic is the Transpolar Drift (TPD). This is an ice and surface ocean current that connects the East Siberian and Laptev seas to the Fram Strait (Morison et al., 2012; Steele et al., 2004) and segregates the surface water of

the Arctic Ocean. The positioning of the TPD can vary between generally along the Lomonosov Ridge in periods with low Arctic Oscillation (AO) index to extending more towards the Chukchi shelf in periods with a high AO (Figure 1)(Morison et al., 2012). As such the relative contributions of waters from the Siberian shelf (Atlantic origin) and Chukchi shelf (Pacific) can vary (Anderson et al., 2004). The TPD carries a clear terrigenous/riverine signal from the Siberian shelves across the Arctic and onwards to the North Atlantic (Anderson et al., 2004; Charette et al., 2020; Williford et al., 2021), but can also entrain a Pacific Water and East Siberian shelf signal, most noticeable as a lack of nitrate and excess silicate (Anderson et al., 2013; Bauch et al., 2011; Jones & Anderson, 1986; McLaughlin et al., 2004), or by having distinctly different DOM properties (Amon et al , 2003; Gonçalves-Araujo et al., 2016; Stedmon et al., 2011a; Williford et al., 2021). These geochemical signals can therefore be used as a tracers of water origin and circulation in the Arctic Ocean.

Much of the empirical knowledge and insight on the origins and characteristics of the Arctic halocline has been based on temperature and salinity profiles (Aagaard et al., 1981; B. Rudels et al., 1996; Steele & Boyd, 1998). This was supplemented with water chemistry measurements, primarily inorganic nutrients, alkalinity, barium and stable oxygen isotopes (Bauch et al., 1995; Guay & Falkner, 1997; Jones & Anderson, 1986). The increasingly widespread deployment of additional biogeochemical sensors (oxygen and a selection of optical probes) on profiling instruments offers higher resolution measurements and an opportunity to further explore processes involved with HL formation, and source fractionation of freshwater distribution (Athanase et al., 2019; Bertosio et al., 2020; Boles et al., 2020; Dmitrenko et al., 2019; Laney et al., 2014). A fraction of the organic compounds present in DOM fluoresce and this can be used as a proxy for dissolved organic carbon in the Arctic (Amon et al., 2003; Gonçalves-Araujo et al., 2016; Guay et al., 1999). This is particularly true for river water entering the Arctic Ocean which has high concentrations of colored and fluorescent DOM (Fichot et al., 2013; Stedmon et al., 2011a; Walker et al., 2013). Fluorescence provides a rapid and sensitive method for characterizing and tracing DOM in the ocean (Stedmon & Nelson, 2015) with the major advantage that it can be measured in situ with readily available single- or multichannel fluorometers (Belzile et al., 2006; Makarewicz et al., 2018). This potentially offers high spatial resolution measurements although the full potential has not been realized due to the lack of a robust and agreed upon cross-sensor calibration procedure. Initial studies from specific instruments have demonstrated their utility for the study of DOM biogeochemistry and water mass tracing in the Arctic Ocean (Amon et al., 2003; Cooper et al., 2005; Dmitrenko et al., 2019; Guay et al., 1999; Williford et al., 2021).

One of the earliest studies measured underway in situ fluorescence at ~50 m depth along the shelf break from the Beaufort Sea towards the Laptev Sea and captured an elevated DOM signal in the Makarov and Amundsen basins from Eurasian river discharge, and a comparatively lower DOM content in the Amerasian Basin (Guay et al., 1999). These findings were subsequently confirmed by Guéguen et al., (2005, 2007) in the Amerasian Basin and Amon et al. (2003) in the Fram Strait. Studies using spectral DOM absorption and fluorescence measured on discrete water samples have been able to further distinguish between DOM in different rivers (Mann et al., 2016; Walker et al., 2013) and differentiate between supply from rivers and shelf sediments (Chen et al., 2016; Gonçalves-Araujo et al., 2016; Guéguen et al., 2007; Stedmon et al., 2011a). What is currently lacking is a comparable calibrated dataset which offers a comprehensive overview, linking the distribution of DOM across the Arctic Ocean to water

masses and their origins. This would provide a baseline from which to detect potential future change and offer an additional tracer for use in model validation.

Here we present a comprehensive intercalibration and analysis of legacy data derived from Ice Tethered Profilers (ITPs) deployed in the central Arctic Ocean which have been equipped with single-channel organic matter fluorometers (often referred to as CDOM or FDOM sensors). Building on the earlier data obtained from the Amerasian Basin (Laney et al., 2014) and expanding the analysis to deeper waters, the data offers unique temporal and spatial coverage of the distribution of DOM in the 800 m below Arctic sea-ice. We demonstrate the utility of high resolution in situ DOM fluorescence as a tracer of Arctic water masses using temperature, salinity and DOM fluorescence. This confirms the close connectivity between the halocline layer composition and linkage to sea-ice formation in shelf waters influenced by river run off. This further infers that winter sea-ice formation on the shelf plays an important role in maintaining stratification in the surface 500 m of much of the Arctic Ocean, which is in turn a major factor controlling sea-ice extent in the central Arctic. Our results also suggest that DOM in the central Arctic Ocean mixes largely conservatively once it has entered the deep and ice-covered central basin and can therefore be used as a tracer of waters of shelf origin and to detect surface freshening due to sea-ice melt from in situ observations.

2 Materials and Methods

The data used for the analysis are summarized in Table 1. It consists of measurements made as part of the Woods Hole Oceanographic Institution ITP program (Krishfield et al., 2008; Toole et al., 2011) (http://www.whoi.edu/itp) and complemented with an ITP from the FRontiers in Arctic marine Monitoring (FRAM) observatory (https://www.awi.de/en/expedition/observatories/ocean-fram.html). These observations are supplemented with data from ship-based profiles from two research cruises: Arctic GEOTRACES GN04 program cruise (PS94, TRANSARC II) with R/V Polarstern and a cruise on the East Greenland Shelf with R/V Dana in 2012 as part of the Danish NAACOS project.

The ITP data are level 3 data products pressure-bin-averaged at 1-db vertical resolution. The ship-based observations are 1 m bin averages. For the ship-based observations, only data for the surface 800 m are included in this analysis as this represented the depths covered by the ITPs. The ITPs were programmed to perform two shallow casts to 200 m then a deep cast to ~750 m. Each profile resulted in an up and a down cast with 6 hour interval in between for the period March to October and 18 hour interval for the remaining months (Laney et al., 2014). The shallowest depth in the processed data on the whole varied between ~5 and 12 m. Figure 1 shows the spatial coverage of the different sensor platforms. In conjunction with the two oceanographic cruises, water samples were collected and used to calibrate the DOM sensors mounted on the ships CTD. ITP93 was deployed during the PS94 cruise and there is an overlap between the first ITP profiles and a ship-based station located at the deployment site. Data from the NAACOS cruise is used to independently verify the applied intercalibration procedure. The profiles from both cruises are included in the data analysis. The instrument package design for ITPs 48-65 and a presentation of the results for the surface 100 m has been published earlier (Laney et al., 2014).

Water samples collected for DOM absorption and fluorescence analysis from the two cruises were filtered through a 0.2 µm Millipore filter cartridge (part # KVGLA04HH3) attached

directly to the rosette sampler bottles once on deck. Then absorption and fluorescence properties of DOM were measured shortly afterwards onboard. DOM fluorescence was measured with a Horiba Aqualog spectrofluorometer and DOM absorption was measured on either a Perkin Elmer Lambda 35 (PS94) or a Shimadzu UVPC2501 (NAACOS) using a 10 cm quartz cuvette and fresh derived pure water (MilliQ with UV lamp) as a blank. Fluorescence data were processed according to community guidelines (Murphy et al., 2010) resulting in inner filter corrected spectra and fluorescence intensities in Raman Units, nm^{-1} (Lawaetz & Stedmon, 2009). The fluorescence intensities at excitation 350 and emission 450 nm were used to calibrate the voltage signal from the CTD mounted fluorometers. It should be noted that the DrHaardt instrument has a slightly different wavelength range (excitation 350-460 nm, emission 550 nm) but that the signal was linearly correlated to the excitation 350 nm and emission 450 nm signal (Figure S1). Fluorescence at these wavelengths (ultraviolet excitation and visible emission) is often referred to as "humic" due to its spectral similarity to soil extracted organic matter. However, it represents a persistent ubiquitous fluorescent signal found in natural waters which originates either from terrestrial organic matter supplied by rivers or from the degradation of marine organic matter (Stedmon & Cory, 2014).

ITP DOM Sensor Intercalibration

The organic matter fluorescence signal from each ITP was first smoothed using a moving average algorithm with a window of 20 m, in order to better recover DOM fluorescence information at the low concentrations characteristic of the central Arctic Ocean. Thereafter the data were checked for fluorescence sensor drift or baseline shifts by plotting the average and standard deviations for each profile for measurements from depths greater than 700 m for temperature (θ), practical salinity (S_p) and DOM fluorescence. At these depths the fluorescence signal was very stable and sensor drift and baseline shifts could be easily identified as either a systematic gradually changing fluorescence signal (typically over first month of a deployment, despite little geographic movement) or a sudden shift (from one day to the next) in the deep-water averages, whilst θ and S_p properties otherwise remained constant. It is likely that these were caused by either gradual biofouling or episodic attachment of matter onto the fluorometer sensor lens. These were corrected for by either subtracting a polynomial fit of the sensor drift or by subtracting a constant value from the remaining data after a given date.

Initial comparison of the baseline corrected ITP data indicated that the fluorometers from each platform required intercalibration (Figure S2). Although the data from the majority of the sensors appear to be either factory or laboratory calibrated pre-deployment to a fluorescence standard (quinine sulfate) there were still notable differences manifesting mostly as different offsets (varying in raw FL units from -10 to +3). The post deployment intercalibration was carried out in two stages. The first step was to calibrate the CTD mounted fluorometer from PS94 to the water samples collected and measured onboard. A linear calibration curve was obtained converting the voltage output signal to fluorescence in Raman Units, [nm^{-1}] (Figure S1).

Secondly θ-S_p plots of individual profiles were examined for a common region in θ-S_p space, representing the same waters were sampled by all platforms and ignoring surface measurements. The region of mixing of lower halocline waters and AW, with salinities ranging from 34.2 to 34.8, was identified to have the best overlap, but the data had to be segregated with

respect to the Eurasian and Amerasian Basins as there were notable differences in θ-S_p between the two. For the Eurasian profiles the lower salinity data were colder and the (high salinity) temperature maximum was warmer (Figure S3) as explained in Rudels et al., (2004). ITP48 sampled both water types during its deployment and could therefore be used to intercalibrate the data between basins.

Data from selected profiles for each ITP were used for the intercalibration to the PS94 CTD mounted calibrated fluorescence (Figure S3). A linear regression between salinity (34.2 to 34.8) and DOM fluorescence was performed for each ITP and used to convert the measured fluorescence to calibrated fluorescence in Raman Units. In order to assess the success of this procedure, two comparisons were made. First, ITP93 was deployed during the PS94 cruise and there was an overlap station from the shipboard CTD on 21 Sep 2015 and the first profile of the ITP on 24 Sep 2015 (Figure S4). Second, the intercalibration approach could be assessed using data from a separate cruise (NAACOS, 2012), calibrated with its own measurements onboard. This was done in DOM-S_p space. Although modifications to polar waters and return AW do occur as it is transported along the Greenland shelf, the clear overlap in the property-property plots offered confidence to the success of the intercalibration of the sensors (Figure S5).

3 Results

The compiled dataset offers coverage of contrasting regions of the Arctic Ocean, namely the Eurasian Basin (Nansen Basin, Gakkel Ridge and Amundsen Basin), the Transpolar Drift (Lomonosov Ridge) and Amerasian Basin (Makarov Basin, Alpha Ridge and Beaufort Gyre) (Figure 1). Histograms of the θ-S_p and DOM-S_p properties of the dataset indicate that the majority of the volume of the upper 800 m in the central Arctic basins has salinities between 32 and 34.8 and potential temperatures ranging from close to their freezing point and increasing to just under 2 °C (Figure 2). The data at lower salinities (<32) stem from the surface 50 m but diverge at a salinity of about 30.5, with Eurasian Basin waters for the most part having temperatures very close to freezing and Beaufort Gyre surface waters being responsible for the warmer temperatures (Figure 2).

At $S_p < 34$ there is considerable spread in DOM fluorescence, revealing two major branches of data (Figure 2), with the remaining data falling between, while the temperature remains comparatively constant and low. The upper branch (higher fluorescence) is an approximately linear extension of the inverse relationship between DOM fluorescence and salinity seen at salinities greater than 34. The lower branch has a local DOM maximum at salinities between 32 and 33, then decreases with decreasing salinity (Figure 2b). The upper branch originates from surface waters in the Eurasian Basin which are influenced by the TPD while the lower branch represents subsurface waters in the Beaufort Gyre originating from the Chukchi Sea and East Siberian Sea (see later analysis).

These patterns are evident in three representative sections shown in Figure 3. The surface waters (upper 50 m) of the Beaufort Gyre (ITP64) are characterized by low salinity and low DOM fluorescence waters with variable temperature (local temperature maxima and minima which are discussed later). Directly below the ice, temperatures are low but increase to a subsurface maximum between 50 and 100 m. Below this is the HL with elevated DOM fluorescence, extending down to approximately 250 m depth. Below the HL, waters mix with warmer and more saline AW with low DOM fluorescence. The other sections shown are from deployments in the Makarov Basin (ITP48) and over the Lomonosov Ridge (ITP93), and capture

the TPD with low salinity and very high DOM fluorescence in the surface 50 m, and also capture an underlying HL with DOM fluorescence intensity comparable to that seen in the Beaufort Gyre HL (Figure 3).

3.1 Archetypical profiles

Figures 4a-c show selected archetypical profiles for θ, S_p and DOM fluorescence in different basins. A profile in the western Nansen Basin (green) has characteristics typical of low DOM fluorescence AW entering the Arctic with surface waters being cooled and diluted by sea-ice melt (Rudels et al., 2004). The winter mixed layer depth is apparent at around 100 m below which there are coincident thermo-, halo- and DOM-clines. In this profile the winter mixed layer is capped by a surface lens with temperatures above freezing for its given salinity (Figure 4d, note deviation from freezing at salinity ~34), and reduced salinity (S_p < 34.35) and DOM fluorescence that has decreased from 0.010 to 0.004 nm^{-1} (Figure 4e) consistent with previous studies (Granskog, et al., 2015; Williford et al., 2021). This likely reflects the addition of summer sea-ice melt water (Bauch et al., 2011; Paffrath et al., 2021) into the surface layer. Sea-ice meltwater contributes comparatively little DOM fluorescence at the wavelengths measured by these sensors and can be assumed to be lower than that found in Atlantic waters (fluorescence <0.01 nm^{-1}) (Granskog, et al., 2015; Stedmon et al., 2011b). In this profile, the warm AW below has the highest temperature, salinity and DOM fluorescence, although the DOM fluorescence is low (<0.01 nm^{-1}) in the upper water column and represents the "pure" AW before it accumulates any DOM signal on its path along the Arctic continental margin (Figure 1). For these waters highest DOM fluorescence was measured at depth (deeper than 800 m, measured using shipboard CTD, not shown), although still considerably lower than the surface DOM maxima from the other regions sampled.

In the profiles in the eastern Amundsen basin (magenta) and in the Makarov basin (black) (Figure 4a-c) the coincident thermo-, halo- and DOM-clines spanning from ~100 to 200 m change character to cover a greater range in salinity and DOM fluorescence, and the direction of the DOM fluorescence gradient changes (now increasing with decreasing salinity) compared to in the Nansen basin. The temperature minimum is at approximately 50 m depth with temperatures very close to freezing (Figure 4d). Below the temperature minimum there is a distinct additional halocline extending to 100 m within which DOM fluorescence decreases essentially linearly with increasing salinity. This reveals that the correlation between DOM and salinity in these waters holds from the base of the PML (temperature minimum) to the AW (Figure 4d and e).

In the surface waters of the Amundsen and Makarov basins there is mixing of underlying halocline waters with sea-ice meltwater in summer. This is most evident for the Amundsen Basin profile (magenta) and at the very surface for the Makarov profile (black). The dilution acts to draw the data off the linear DOM-S_p mixing line (compare magenta and black profiles in Figure 4e) and towards a lower salinity and DOM fluorescence water type.

In Figure 4 two profiles from the Beaufort Gyre are shown (cyan and red). Although the depth distributions differ (Figure 4a-c), the water mass characteristics (S_p and DOM fluorescence in particular) of these two profiles overlap very closely (Figure 4d & e). The main deviation is in the surface 50 m with salinities below 32 where temperatures are considerably warmer in the profile that originates from closer to the Alaskan shelf (cyan, from June 2013) than in the central basin (red, from September 2012). In these profiles an additional thick upper layer of the UHC is evident underneath the PML, with salinities ranging from approximately 32 to 33. This layer has

an intermediate DOM fluorescence which is less than half that found at comparable salinities in the Makarov Basin profile (black) but still much higher than that found in AW (green). The DOM-S_p diagram reveals that this layer sits above the LHC waters (Figure 4e).

In the region of the Alpha Ridge (Figure 4, blue), surface waters are diluted tending towards similar values for salinity and DOM fluorescence as that seen in the Beaufort Gyre (Figure 4, red and cyan). Below this, the water column has similar properties to the Makarov and Amundsen basin (black and magenta), with high DOM fluorescence and near freezing temperatures. At 90-150 m depth there is an intrusion of intermediate fluorescence DOM signal associated with UHC from the Beaufort Gyre (Figure 4e).

For comparison, a profile from the East Greenland shelf (brown) is also shown in Figure 4. At salinities between 32 and 33 and at ~34.8 there is clear overlap in θ-S_p and DOM-S_p space with data from the central Arctic Ocean. Waters with these properties correspond to Beaufort Gyre upper halocline and Atlantic waters, respectively. However, it should be noted that this profile does not represent a widespread or typical signal for much of the East Greenland shelf. At other stations, not highlighted here, there is no overlap with the UHC waters, but rather a more predominant signal from the Siberian shelf contribution is apparent (Amon et al., 2003; Gonçalves-Araujo et al., 2016).

3.2 Characteristics of the DOM maximum, temperature maximum and temperature minimum

The following section presents the results of an analysis of the properties and location of three distinct features in the profiles: the DOM fluorescence maximum, the temperature maximum and the temperature minimum. For each of the more than 5000 profiles the specific depth of the above features was found and histograms of the water properties at these depths were generated (Figure 5-7). These indicated the presence of distinct sub-groups of data. In order to highlight these groups and aid in determination of the origins of the measurements contributing to them, arbitrary distinctions are made depending on either salinity, DOM fluorescence intensity or deviation from freezing temperature (see figure legends for boundaries of these arbitrary groups). The emphasis should be on the shape of the histograms (with distinct or overlapping distributions). The grouping allocated, indicated in the figures by different colors, serve only to facilitate interpretation.

Figure 5 shows histograms of water properties at the DOM fluorescence maxima for each profile for halocline waters (S_p 31-34). The histograms reduce the data considerably as there is now only one data point per profile. This facilitates isolating the characteristics of different high intensity DOM sources, in particular in the range of halocline salinities across the Arctic. It is clear that DOM fluorescence maxima in the Arctic Ocean can be grouped into two based on their temperature (or rather deviation from freezing temperature, DFT): either essentially at seawater freezing temperatures (red group in Figure 5e) or centered around 0.4 °C above freezing (Figure 5e). The waters with the coldest (and closest to freezing) temperatures (red in Figure 5c) have the highest DOM fluorescence (>0.030 nm^{-1} with a tail extending up to 0.0888 nm^{-1}). Similarly, there is clear segregation with respect to depth. The DOM fluorescence maxima tend to be either at the surface (red group, with corresponding highest DOM fluorescence) or much deeper (between 100 and 250 m; Figure 5d) which is typically observed for the Beaufort Gyre stations (west of 100 °W). The latter has lower DOM fluorescence centered around 0.03 nm^{-1} (blue and yellow data in Figure 5c).

The surface maxima (red, Figure 5) can also be segregated to maxima at depths <25 m, corresponding to profiles in the TPD, and maxima positioned slightly deeper immediately below

the PML at approximately 60 m (corresponding to the HL in the Eurasian Basin). These data span a range in salinities from 31 to 33.2 and originate from profiles taken in the Amundsen Basin, Lomonosov Ridge and near the North Pole. There is also a significant negative linear correlation between DOM fluorescence intensity and salinity for these samples ($r=-0.72$, $p<0.01$).

The lower DOM fluorescence intensity group (<0.030 nm^{-1}) could be separated further into two, based on salinity, with an apparent threshold between them of 33.2 (blue and yellow in Figure 5). Although there was a high degree of overlap in temperature (Figure 5b), typically ranging from 0.3 to 0.75 °C DFT, a two sample t-test indicated that there was a significant difference ($p<0.01$) with the higher salinity group (yellow) being significantly warmer. These groups also differed slightly in position in the water column, with the lower salinity group (blue) slightly shallower (mean depth 155 m) than the higher salinity group (mean depth 182 m, Figure 5d).

Another prominent feature of the water column in the Arctic Ocean is the intermediate and deep temperature maxima which trace the warm Pacific and Atlantic waters, respectively, that enter the Arctic (Jackson et al., 2010; Korhonen et al., 2013). In Figure 6 histograms of the properties at the temperature maximum are shown but grouped based on their salinity and depth. For this analysis, only profiles with a distinct deep θ maximum were included (i.e., shallow ITP profiles to ~200 m where temperature was still increasing with depth were excluded). Here, one can identify three groups with contrasting θ, S_p and DOM fluorescence (Figure 6). The temperature maximum of the AW inflow waters (shown in blue) are widespread across the basin, and are typically found at depths between 200 and 350 m, at S_p of ~34.9 and with θ ranging between 0.5 and 2 °C. These waters are characterized by low DOM fluorescence (~0.01 nm^{-1}). In the Amerasian Basin, salinity at the deep (AW) temperature maximum (0.7-0.9 °C), is slightly lower (34.8), but has comparably low DOM fluorescence of ~0.01 nm^{-1} (shown in yellow, Figure 6) and is found deeper in the water column (350-400 m). The third group, shown in red in Figure 6, corresponds to warm near surface waters in the Amerasian Basin that have entered through the Bering Strait, and been modified by warming and sea-ice melt. These waters have comparatively higher DOM fluorescence, centered around 0.017 nm^{-1}, compared to the deep temperature maxima (~0.01 nm^{-1}).

An analysis of the properties at the temperature minimum also revealed distinct groups based on temperature and salinity (Figure 7). The deep temperature minimum (typically >100 m) in the Amerasian Basin differed from the others by having temperatures that deviated more than 0.2 °C from seawater freezing (blue) and a DOM fluorescence of 0.028 nm^{-1}. In surface waters the temperature minima were largely within 0.2 °C from seawater freezing but could be segregated based on salinity. The lowest salinity temperature minimum ($S<29$) was restricted to upper surface waters and the majority of the data had low DOM fluorescence (<0.012 nm^{-1}). At salinities between 29.5 and 32 two distinct groups could be identified, a lower salinity group with low DOM fluorescence (~0.02 nm^{-1}, S_p 30-31) and a higher salinity group with a higher DOM fluorescence (~0.03 nm^{-1}, S_p 32-33). Both of these were found at depths between 40-70 m.

4 Discussion

Figure 8 shows the average properties of each of the identified end members from the DOM and temperature maxima and temperature minima, superimposed on all the data (complete profiles) in θ-S_p (Figure 8a) and DOM-S_p (Figure 8b) space. These are calculated across all profiles. It is

evident that the DOM fluorescence signal offers an additional parameter from which to separate the properties of the surface waters of the Arctic Ocean (S_p<34 and θ<0), where temperatures are often low and overlap considerably despite different water mass origins. In particular, the data can resolve patterns in the UHC, while the changes in the DOM fluorescence of AW are minor as it propagates through the Arctic Ocean.

4.1 Oceanic DOM signal associated with AW branches.

The DOM fluorescence signal found in the temperature maximum waters originating from AW has comparable intensity to that found in earlier studies for ocean waters without a notable influence from terrestrial input (Jørgensen et al., 2011; Zabłocka et al., 2020). This represents a background recalcitrant oceanic signal produced from the long term microbial and photochemical processing of marine organic matter in the world ocean (Jørgensen et al., 2011, 2014; Yamashita & Tanoue, 2008). AW enters the Arctic through the Fram Strait or via the Barents Sea (Rudels et al., 2004). The Fram Strait and Barents Sea contributions to these surface waters are cooled and diluted by sea-ice melt. This further decreases the DOM fluorescence signal brought with it as seen in the Nansen Basin profile in Figure 4. At certain locations microbial activity in sea-ice can result in the production and accumulation of fluorescent DOM in sea-ice brines (Stedmon et al., 2011b). However, this fluorescence is dominated by DOM with an ultraviolet fluorescence (emission < 400 nm) (Granskog, et al., 2015) which represents a transient labile organic matter signature. When this material is introduced into surface waters as a result of sea-ice melt, it is susceptible to mineralization by microbes. Visible wavelength fluorescence (emission), such as that measured by the sensors deployed in this study, can also be released during sea-ice melt but the signal intensities are lower, typically 0.005 nm^{-1} (Stedmon et al., 2011b), but more resistant to degradation, and can therefore result in a slight reduction in the surface AW signal.

Atlantic waters flow eastwards along the Siberian continental slope forming the Arctic Circumpolar Boundary Current (ACBC) (Aksenov et al., 2011). The saline temperature maximum group identified in Figure 6 trace the path of AW starting shallow (200-350 m) and with variable warm temperatures in the Eurasian Basin (0.5-2 °C) (blue in Figure 6) and ending as a deeper (400-500 m) and colder temperature maxima (0.7-0.9 °C) in the Amerasian Basin (yellow in Figure 6) which is much more homogenous with respect to temperature and only slightly less saline (S_p~34.8). The DOM fluorescence in these waters does not change reflecting its refractory nature, similar AW origins, and indicating no entrainment of riverine or shelf sediment organic matter signal during its passage. This has also been confirmed earlier using terrestrial plant biomarker lignin measurements (Kaiser et al., 2017).

The waters of the LHC are defined as having salinities greater than 34 and temperatures below 0 °C (Korhonen et al., 2013; Rudels et al., 1996). These originate from the freshening and cooling of AW after entering the Arctic Ocean north of Svalbard or via the Barents Sea. As a result, one would expect them to have a very low DOM fluorescence (as discussed above). The majority of the water sampled with a salinity greater than 34 had higher DOM fluorescence than expected for AW, 0.03 nm^{-1} rather than 0.01 nm^{-1}, (Figure 8) and was positioned on the Siberian shelf–AW mixing line. Two regions are thought to contribute to the formation of the LHC, and these results imply that the open ocean convective contribution to the LHC from winter waters in the Nansen Basin (Rudels et al., 1996) may be of minor importance in the waters sampled here. The distinct elevated DOM fluorescence emphasizes the importance of the Barents Sea branch entering via the Kara Sea where there is a terrestrial DOM contribution from Ob and Yenisei

rivers. Almost all of the Atlantic-derived water beyond the Lomonosov Ridge is thought to have come through the Barents Sea (Rudels et al., 1996) but the data here indicate a dominance of this water also in the Amundsen Basin with little evidence for the Nansen Basin contribution along the tracks covered by the ITPs and shipboard measurements.

4.2 Shelf DOM signals

A branch of the Barents Sea supply of AW contains a contribution from the Norwegian Coastal Current and flows along the Siberian shelf and slope (Osadchiev et al., 2020; Rudels et al., 2004). During this passage it collects freshwater (Bauch et al., 2014) and DOM from Siberian rivers (Kaiser et al., 2017). Export of these waters northwards off the shelf and mixing with underlying AW results in the negative correlation observed between DOM fluorescence and salinity (black line in Figure 4e). The analysis of the properties of the DOM fluorescence maxima identified three distinct groups with shelf origins. This demonstrates that different shelf components are detectable in the HL as has been demonstrated based on neodymium (Nd) isotopes for the Lapev and Kara seas components within the TPD (Paffrath et al., 2021). The group with the highest DOM fluorescence values (red in Figure 5) overlap in salinity, temperature and depth with previously defined Lower Salinity Halocline Waters (LSHW) (Bauch et al., 2014; Bauch et al., 2011). These surface waters originate from the Laptev and East Siberian seas (Bauch et al., 2014) and are exported northwards off shelf forming the surface waters of the TPD (Rudels et al., 1999) and carry with them a high terrigenous DOM fluorescence (Charette et al., 2020; Williford et al., 2021) and intermediate silicate concentrations (Anderson et al., 2017) from Siberian river run off. DOM fluorescence at salinities of 30 for shelf waters near the Lena River have been reported to be around 0.1 nm^{-1} (Gonçalves-Araujo et al., 2015) and this aligns well if one extrapolates the mixing curve for the Makarov Basin (black) shown in Figure 4. Measurement of the terrestrial plant biomarker lignin has also shown that the DOM in these waters originates from the Ob, Yenisei and Lena rivers (Kaiser et al., 2017; Williford et al., 2021). The strong linear correlation with salinity indicates conservative mixing between LSHW of the TPD with the underlying AW at the temperature maximum. The results also show that in places (Amerasian Basin side of TDP) this can be subducted below lower salinity surface water from the Beaufort Gyre (Figure 4, blue; Figure 5, red).

LSHW temperatures are very close to freezing (for the most part within 0.3 °C of freezing for their given salinity), which confirms the role that brine release during sea-ice formation has on shaping the properties of these waters (Aagaard et al., 1981). Mixing with sea-ice melt water is apparent at the very surface of the profiles where both DOM fluorescence and salinity is reduced (black profile in Figure 4) and is consistent with a recent study with extensive coverage of the Siberian shelf water (Hölemann et al., 2021).

The highest salinity DOM fluorescence maximum group (S_p 33.7, Figure 8) lies on the LSHW–AW mixing line, but is found at depths greater than 150 m (yellow in Figure 5), and slightly warmer (~0.5 °C above seawater freezing). The fact that these data lie directly on this mixing line hints to the fact that it is also formed on the Siberian shelf but contains a greater contribution of Atlantic water. Although salinities range between 33.4-34.2, its depth and location indicate that it represents part of the LHC in the Amerasian Basin.

A third group with similar DOM fluorescence but lower salinities (mean S_p 32.9) was also identified (blue in Figure 5). These waters have temperatures approximately 0.4 °C above seawater freezing, and represent Pacific inflow waters passing across the Chukchi Sea (Guéguen

et al., 2012; Jones & Anderson, 1986; Stedmon et al., 2011a) or East Siberian shelf water (Anderson et al., 2017), which have accumulated DOM largely from shelf sediments. This is confirmed by the fact that near identical water column characteristics can be found in the Beaufort Gyre profiles (compare red and cyan data in Figure 4). As these waters pass over the shelf, seasonal sea-ice formation (Shimada, 2005) acts to drive temperatures close to freezing and there is a DOM contribution from marine organic matter degradation in shelf sediments. Here the DOM released clearly differs in character from riverine material and likely originated from the degradation of marine organic matter (Stedmon et al., 2011a). This aligns with the nutrient signal reported for these waters (Anderson et al., 2017; Jones & Anderson, 1986). In the Amerasian Basin, these waters lie above the LHC from the Eurasian Basin (red and cyan data in Figure 3) however at the Alpha Ridge (blue profile in Figure 3) one can find contribution from all three DOM groups with shelf UHC water inserted between LSHW and LHC. This fits with earlier observations in the central Arctic (McLaughlin et al., 2004; Shimada, 2005; Woodgate et al., 2007) and from the Wandel Sea off Northeast Greenland (Dmitrenko et al., 2019). Waters with similar properties, overlapping in θ-S_p and DOM-S_p space, were also identified by the analysis of the temperature minimum (Figure 8, blue and black points at S of ~33). The temperature and salinity confirm its origin as PWW.

The shallow temperature maximum <100m in the Amerasian Basin represents the Pacific inflow as PSW (Rudels et al., 2004). This was distinguished as a group of data with salinities between 30 and 32 and intermediate DOM fluorescence (red in Figure 8). The location of these data in DOM-S space indicate that they represent a dilution of the PWW (in both S and DOM), with a contribution of freshwater from ice melt.

The characteristics of the waters contributing to the variability in DOM fluorescence in the Arctic Ocean can be summarized as follows. At the surface low salinity (S<32.5) and high DOM fluorescence waters (LSHW) that originate on the Siberian shelf and are exported northwards with the TPD. Below this are the waters of the Atlantic derived LHC which have intermediate DOM fluorescence indicating that they have also entrained terrestrial DOM from the Siberian shelf during their formation before exported northwards and subducted. In addition to being exported northwards together with the TPD a contribution is also diverted into the Beaufort Gyre where it supplies terrestrial DOM into the LHC beneath the UHC. The UHC, despite having a comparable DOM fluorescence to the LHC, has a lower salinity and collects its (marine/shelf) DOM signal from the Chukchi shelf and East Siberian Sea. All three components of HL can be captured in profiles near Alpha Ridge (e.g. Figure 4) and in the Fram Strait (not shown). While the signal at the surface from the TPD, is diluted with sea-ice melt on its journey out of the Arctic, the signals from the Pacific and Atlantic HL at depth are retained and identifiable all the way to the East Greenland shelf. This is supported by comparing the data collected from the Beaufort Gyre (cyan and red, Figure 4e) with measurements from the East Greenland Shelf in DOM-S space (brown, Figure 4e), and supports earlier evidence based on water samples (Gonçalves-Araujo et al., 2016).

5 Conclusions and outlook

The results shown indicate that two major freshwater sources to the Arctic, river discharge and Pacific water, have clear and distinguishable DOM fluorescence signals associated with them. This confirms earlier findings based on more in-depth water sample analysis in selected Arctic regions (Amon et al., 2003; Gonçalves-Araujo et al., 2016; Stedmon et al., 2011a; Williford et

al., 2021) but here the high temporal and spatial resolution of in situ measurements throughout the Arctic Ocean complements the regional studies with better analytical resolution of laboratory measurements.

DOM fluorescence at the wavelengths measured by these sensors (ultraviolet excitation and visible wavelength fluorescence), behaves largely conservatively relative to salinity during sea-ice formation and subsequent brine rejection (Stedmon et al., 2011b). The released brine (with slightly elevated salinities and DOM fluorescence, and near seawater freezing temperatures) contributes to the formation of shelf waters that feed the halocline. While Siberian shelf water contributes terrestrial DOM into the LHC, the water from the Chukchi shelf contributes with marine DOM likely released from sediment below the highly productive Chukchi shelf. Although high salinity waters of the LHC can contain a contribution from winter mixing in the Nansen Basin, the evidence shown here indicates widespread dominance of shelf water sources elsewhere.

In the upper 300 m of the Beaufort Gyre salinity profiles reflect the considerable storage of freshwater in the region. Here DOM profiles from automated platforms may provide additional insight to the source of the freshwater. River water and Pacific water will be associated with high DOM fluorescence while accumulation of sea-ice melt will dilute DOM fluorescence (resulting in positive correlation with salinity). The DOM fluorescence-S_p diagrams clearly indicate an accumulation of sea-ice melt in the surface 50 m (S_p below 30). Combined with additional biogeochemical sensors such as nitrate and oxygen (Athanase et al., 2019), DOM fluorescence measurements provide an opportunity to fractionate freshwater contributions based on in situ measurements alone. In addition, multi-channel in situ fluorometers would be able to better differentiate between Arctic DOM sources as they differ in their spectral properties (Gonçalves-Araujo et al., 2016; Makarewicz et al., 2018), while spectral absorption sensors such as those used for nitrate can potentially provide high resolution estimates of DOC (Gonçalves-Araujo et al., 2020). Surface DOM measurements can easily distinguish the frontal regions on either side of the TPD, and in the vertical provides a powerful tool to guide water sampling of other tracers in the water column (Charette et al., 2020; Williford et al., 2021). This offers a valuable and currently underutilized additional tracer for deciphering Arctic circulation and freshwater distribution. Some of these questions are addressed by a parallel paper in this special issue by Williford et al.

Acknowledgments, Samples, and Data

Danish Strategic Research Council for the NAACOS project (grant no. 10-093903), the Danish Center for Marine Research (grant no. 2012-01). C. A. S. has received funding from the Independent Research Fund Denmark Grant No. 9040-00266B. Funding for R.M.W.A. came from the US NSF, Arctic Natural Science program grant 1504469. RG-A has received funding from the European Union's Horizon 2020 research and innovation program under the Marie Skłodowska-Curie Grant Agreement No. 839311. ITP93 and part of the work by MH and BR were a contribution to the Helmholtz society strategic investment Frontiers in Arctic Marine monitoring (FRAM). The work of BR is a contribution to the cooperative projects Regional Atlantic Circulation and global Change (RACE) grant #03F0824E funded by the German Ministry of Science and Education (BBMF) and Advective Pathways of nutrients and key Ecological substances in the Arctic (APEAR) grants NE/R012865/1,NE/R012865/2 and #03V01461, part of the Changing Arctic Ocean programme, jointly funded by the UKRI Natural

Environment Research Council (NERC) and the BMBF. Support for Krishfield was made possible by grants from the NSF Arctic Observing Network program (PLR-1303644 and OPP-1756100). We thank the FRAM (Helmholtz infrastructure initiative "Frontiers of Arctic Marine Monitoring") associated technicians, engineers, scientists and administrators as well as the captains, crews, and chief scientists of R/V Polarstern and R/V Dana who were all instrumental in making these observations possible. We also thank L. G. Anderson for a constructive review of the manuscript. The complete dataset is available for download from DTU data archive doi.org/10.11583/DTU.14827581.

References

Aagaard, K., Coachman, L. K., & Carmack, E. (1981). On the halocline of the Arctic Ocean. *Deep Sea Research Part A. Oceanographic Research Papers*, *28*(6), 529–545. https://doi.org/10.1016/0198-0149(81)90115-1

Aksenov, Y., Ivanov, V. V., Nurser, A. J. G., Bacon, S., Polyakov, I. V., Coward, A. C., et al. (2011). The Arctic Circumpolar Boundary Current. *Journal of Geophysical Research: Oceans*, *116*(C9). https://doi.org/10.1029/2010JC006637

Amon, R. M. W., Budéus, G., & Meon, B. (2003). Dissolved organic carbon distribution and origin in the Nordic Seas: Exchanges with the Arctic Ocean and the North Atlantic. *Journal of Geophysical Research: Oceans*, *108*(C7). https://doi.org/10.1029/2002JC001594

Amon, R. M. W., Rinehart, A. J., Duan, S., Louchouarn, P., Prokushkin, A., Guggenberger, G., et al. (2012). Dissolved organic matter sources in large Arctic rivers. *Geochimica et Cosmochimica Acta*, *94*, 217–237. https://doi.org/10.1016/j.gca.2012.07.015

Anderson, L. G., & Amon, R. M. W. (2015). DOM in the Arctic Ocean. In *Biogeochemistry of Marine Dissolved Organic Matter* (pp. 609–633). Elsevier. https://doi.org/10.1016/B978-0-12-405940-5.00014-5

Anderson, L. G., P. Jones, E., Lindegren, R., Rudels, B., & Sehlstedt, P.-I. (1988). Nutrient regeneration in cold, high salinity bottom water of the Arctic shelves. *Continental Shelf Research*, *8*(12), 1345–1355. https://doi.org/10.1016/0278-4343(88)90044-1

Anderson, L. G., Jutterström, S., Kaltin, S., Jones, E. P., & Björk, G. (2004). Variability in river runoff distribution in the Eurasian Basin of the Arctic Ocean. *Journal of Geophysical Research: Oceans*, *109*(C1). https://doi.org/10.1029/2003JC001773

645 Anderson, L. G., Andersson, P. S., Björk, G., Peter Jones, E., Jutterström, S., & Wåhlström, I. (2013). Source and
646 formation of the upper halocline of the Arctic Ocean: Arctic Ocean upper halocline. *Journal of*
647 *Geophysical Research: Oceans*, *118*(1), 410–421. https://doi.org/10.1029/2012JC008291
648 Anderson, L. G., Björk, G., Holby, O., Jutterström, S., Mörth, C. M., O'Regan, M., et al. (2017). Shelf–Basin
649 interaction along the East Siberian Sea. *Ocean Science*, *13*(2), 349–363. https://doi.org/10.5194/os-13-349-
650 2017
651 Athanase, M., Sennéchael, N., Garric, G., Koenig, Z., Boles, E., & Provost, C. (2019). New Hydrographic
652 Measurements of the Upper Arctic Western Eurasian Basin in 2017 Reveal Fresher Mixed Layer and
653 Shallower Warm Layer Than 2005–2012 Climatology. *Journal of Geophysical Research: Oceans*, *124*(2),
654 1091–1114. https://doi.org/10.1029/2018JC014701
655 Bauch, D., Torres-Valdes, S., Polyakov, I., Novikhin, A., Dmitrenko, I., McKay, J., & Mix, A. (2014). Halocline
656 water modification and along-slope advection at the Laptev Sea continental margin. *Ocean Science*, *10*(1),
657 141–154. https://doi.org/10.5194/os-10-141-2014
658 Bauch, Dorothea, Schlosser, P., & Fairbanks, R. G. (1995). Freshwater balance and the sources of deep and bottom
659 waters in the Arctic Ocean inferred from the distribution of H218O. *Progress in Oceanography*, *35*(1), 53–
660 80.
661 Bauch, D., van der Loeff, M. R., Andersen, N., Torres-Valdes, S., Bakker, K., & Abrahamsen, E. P. (2011). Origin
662 of freshwater and polynya water in the Arctic Ocean halocline in summer 2007. *Progress in*
663 *Oceanography*, *91*(4), 482–495. https://doi.org/10.1016/j.pocean.2011.07.017
664 Belzile, C., Roesler, C. S., Christensen, J. P., Shakhova, N., & Semiletov, I. (2006). Fluorescence measured using
665 the WETStar DOM fluorometer as a proxy for dissolved matter absorption. *Estuarine, Coastal and Shelf*
666 *Science*, *67*(3), 441–449. https://doi.org/10.1016/j.ecss.2005.11.032
667 Bertosio, C., Provost, C., Sennéchael, N., Artana, C., Athanase, M., Boles, E., et al. (2020). The Western Eurasian
668 Basin Halocline in 2017: Insights From Autonomous NO Measurements and the Mercator Physical System.
669 *Journal of Geophysical Research: Oceans*, *125*(7), e2020JC016204. https://doi.org/10.1029/2020JC016204
670 Boles, E., Provost, C., Garçon, V., Bertosio, C., Athanase, M., Koenig, Z., & Sennéchael, N. (2020). Under-Ice
671 Phytoplankton Blooms in the Central Arctic Ocean: Insights From the First Biogeochemical IAOOS

672 Platform Drift in 2017. *Journal of Geophysical Research: Oceans*, *125*(3), e2019JC015608.
673 https://doi.org/10.1029/2019JC015608
674 Charette, M. A., Kipp, L. E., Jensen, L. T., Dabrowski, J. S., Whitmore, L. M., Fitzsimmons, J. N., et al. (2020). The
675 Transpolar Drift as a Source of Riverine and Shelf-Derived Trace Elements to the Central Arctic Ocean.
676 *Journal of Geophysical Research: Oceans*, *125*(5), e2019JC015920. https://doi.org/10.1029/2019JC015920
677 Chen, M., Kim, J.-H., Nam, S.-I., Niessen, F., Hong, W.-L., Kang, M.-H., & Hur, J. (2016). Production of
678 fluorescent dissolved organic matter in Arctic Ocean sediments. *Scientific Reports*, *6*(1), 39213.
679 https://doi.org/10.1038/srep39213
680 Coachman, L. K., & Aagaard, K. (1974). Physical Oceanography of Arctic and Subarctic Seas. In Y. Herman (Ed.),
681 *Marine Geology and Oceanography of the Arctic Seas* (pp. 1–72). Berlin, Heidelberg: Springer.
682 https://doi.org/10.1007/978-3-642-87411-6_1
683 Coachman, L. K., & Barnes, C. A. (1961). The Contribution of Bering Sea Water to the Arctic Ocean. *Arctic*, *14*(3),
684 147–161.
685 Codispoti, L. A., Flagg, C., Kelly, V., & Swift, J. H. (2005). Hydrographic conditions during the 2002 SBI process
686 experiments. *Deep Sea Research Part II: Topical Studies in Oceanography*, *52*(24–26), 3199–3226.
687 https://doi.org/10.1016/j.dsr2.2005.10.007
688 Cooper, L. W., Benner, R., McClelland, J. W., Peterson, B. J., Holmes, R. M., Raymond, P. A., et al. (2005).
689 Linkages among runoff, dissolved organic carbon, and the stable oxygen isotope composition of seawater
690 and other water mass indicators in the Arctic Ocean. *Journal of Geophysical Research: Biogeosciences*,
691 *110*(G2), n/a-n/a. https://doi.org/10.1029/2005JG000031
692 Dmitrenko, I. A., Kirillov, S. A., Ivanov, V. V., Woodgate, R. A., Polyakov, I. V., Koldunov, N., et al. (2009).
693 Seasonal modification of the Arctic Ocean intermediate water layer off the eastern Laptev Sea continental
694 shelf break. *Journal of Geophysical Research: Oceans*, *114*(C6). https://doi.org/10.1029/2008JC005229
695 Dmitrenko, I. A., Ivanov, V. V., Kirillov, S. A., Vinogradova, E. L., Torres-Valdes, S., & Bauch, D. (2011).
696 Properties of the Atlantic derived halocline waters over the Laptev Sea continental margin: Evidence from
697 2002 to 2009. *Journal of Geophysical Research: Oceans*, *116*(C10). https://doi.org/10.1029/2011JC007269

698 Dmitrenko, I. A., Kirillov, S. A., Rudels, B., Babb, D. G., Myers, P. G., Stedmon, C. A., et al. (2019). Variability of
699 the Pacific-Derived Arctic Water Over the Southeastern Wandel Sea Shelf (Northeast Greenland) in 2015-
700 2016. *Journal of Geophysical Research: Oceans*. https://doi.org/10.1029/2018JC014567
701 Fichot, C. G., Kaiser, K., Hooker, S. B., Amon, R. M. W., Babin, M., Bélanger, S., et al. (2013). Pan-Arctic
702 distributions of continental runoff in the Arctic Ocean. *Scientific Reports*, *3*(1).
703 https://doi.org/10.1038/srep01053
704 Gonçalves-Araujo, R., Stedmon, C. A., Heim, B., Dubinenkov, I., Kraberg, A., Moiseev, D., & Bracher, A. (2015).
705 From Fresh to Marine Waters: Characterization and Fate of Dissolved Organic Matter in the Lena River
706 Delta Region, Siberia. *Frontiers in Marine Science*, *2*. https://doi.org/10.3389/fmars.2015.00108
707 Gonçalves-Araujo, R., Granskog, M. A., Bracher, A., Azetsu-Scott, K., Dodd, P. A., & Stedmon, C. A. (2016).
708 Using fluorescent dissolved organic matter to trace and distinguish the origin of Arctic surface waters.
709 *Scientific Reports*, *6*(1). https://doi.org/10.1038/srep33978
710 Gonçalves-Araujo, R., Stedmon, C. A., Steur, L. de, Osburn, C. L., & Granskog, M. A. (2020). A Decade of Annual
711 Arctic DOC Export With Polar Surface Water in the East Greenland Current. *Geophysical Research*
712 *Letters*, *47*(20), e2020GL089686. https://doi.org/10.1029/2020GL089686
713 Granskog, M. A., Pavlov, A. K., Sagan, S., Kowalczuk, P., Raczkowska, A., & Stedmon, C. A. (2015). Effect of
714 sea-ice melt on inherent optical properties and vertical distribution of solar radiant heating in Arctic surface
715 waters. *Journal of Geophysical Research: Oceans*, *120*(10), 7028–7039.
716 https://doi.org/10.1002/2015JC011087
717 Granskog, M. A., Nomura, D., Müller, S., Krell, A., Toyota, T., & Hattori, H. (2015). Evidence for significant
718 protein-like dissolved organic matter accumulation in Sea of Okhotsk sea ice. *Annals of Glaciology*, *56*(69),
719 1–8. https://doi.org/10.3189/2015AoG69A002
720 Guay, Christopher K., Klinkhammer, G. P., Falkner, K. K., Benner, R., Coble, P. G., Whitledge, T. E., et al. (1999).
721 High-resolution measurements of dissolved organic carbon in the Arctic Ocean by *in situ* fiber-optic
722 spectrometry. *Geophysical Research Letters*, *26*(8), 1007–1010. https://doi.org/10.1029/1999GL900130
723 Guay, C.K., & Kenison Falkner, K. (1997). Barium as a tracer of Arctic halocline and river waters. *Deep Sea*
724 *Research Part II: Topical Studies in Oceanography*, *44*(8), 1543–1569. https://doi.org/10.1016/S0967-
725 0645(97)00066-0

Guéguen, C., Guo, L., & Tanaka, N. (2005). Distributions and characteristics of colored dissolved organic matter in the Western Arctic Ocean. *Continental Shelf Research*, *25*(10), 1195–1207. https://doi.org/10.1016/j.csr.2005.01.005

Guéguen, C., Guo, L., Yamamoto-Kawai, M., & Tanaka, N. (2007). Colored dissolved organic matter dynamics across the shelf-basin interface in the western Arctic Ocean. *Journal of Geophysical Research: Oceans*, *112*(C5). https://doi.org/10.1029/2006JC003584

Haine, T. W. N., Curry, B., Gerdes, R., Hansen, E., Karcher, M., Lee, C., et al. (2015). Arctic freshwater export: Status, mechanisms, and prospects. *Global and Planetary Change*, *125*, 13–35. https://doi.org/10.1016/j.gloplacha.2014.11.013

Hardison, A. K., McTigue, N. D., Gardner, W. S., & Dunton, K. H. (2017). Arctic shelves as platforms for biogeochemical activity: Nitrogen and carbon transformations in the Chukchi Sea, Alaska. *Deep Sea Research Part II: Topical Studies in Oceanography*, *144*, 78–91. https://doi.org/10.1016/j.dsr2.2017.08.004

Hölemann, J. A., Juhls, B., Bauch, D., Janout, M., Koch, B. P., & Heim, B. (2021). The impact of land-fast ice on the distribution of terrestrial dissolved organic matter in the Siberian Arctic shelf seas. *Biogeosciences Discussions*, 1–30. https://doi.org/10.5194/bg-2020-462

Holmes, R. M., McClelland, J. W., Peterson, B. J., Tank, S. E., Bulygina, E., Eglinton, T. I., et al. (2012). Seasonal and Annual Fluxes of Nutrients and Organic Matter from Large Rivers to the Arctic Ocean and Surrounding Seas. *Estuaries and Coasts*, *35*(2), 369–382. https://doi.org/10.1007/s12237-011-9386-6

Jackson, J. M., Carmack, E. C., McLaughlin, F. A., Allen, S. E., & Ingram, R. G. (2010). Identification, characterization, and change of the near-surface temperature maximum in the Canada Basin, 1993–2008. *Journal of Geophysical Research: Oceans*, *115*(C5). https://doi.org/10.1029/2009JC005265

Jones, E. P., & Anderson, L. G. (1986). On the origin of the chemical properties of the Arctic Ocean halocline. *Journal of Geophysical Research*, *91*(C9), 10759. https://doi.org/10.1029/JC091iC09p10759

Jørgensen, L., Stedmon, C. A., Kragh, T., Markager, S., Middelboe, M., & Søndergaard, M. (2011). Global trends in the fluorescence characteristics and distribution of marine dissolved organic matter. *Marine Chemistry*, *126*(1–4), 139–148. https://doi.org/10.1016/j.marchem.2011.05.002

752 Jørgensen, L., Stedmon, C. A., Granskog, M. A., & Middelboe, M. (2014). Tracing the long-term microbial
753 production of recalcitrant fluorescent dissolved organic matter in seawater. *Geophysical Research Letters*,
754 *41*(7), 2481–2488. https://doi.org/10.1002/2014GL059428
755 Kaiser, K., Benner, R., & Amon, R. M. W. (2017). The fate of terrigenous dissolved organic carbon on the Eurasian
756 shelves and export to the North Atlantic. *Journal of Geophysical Research: Oceans*, *122*(1), 4–22.
757 https://doi.org/10.1002/2016JC012380
758 Korhonen, M., Rudels, B., Marnela, M., Wisotzki, A., & Zhao, J. (2013). Time and space variability of freshwater
759 content, heat content and seasonal ice melt in the Arctic Ocean from 1991 to 2011. *Ocean Science*, *9*(6),
760 1015–1055. https://doi.org/10.5194/os-9-1015-2013
761 Krishfield, R., Toole, J., Proshutinsky, A., & Timmermans, M.-L. (2008). Automated Ice-Tethered Profilers for
762 Seawater Observations under Pack Ice in All Seasons. *Journal of Atmospheric and Oceanic Technology*,
763 *25*(11), 2091–2105. https://doi.org/10.1175/2008JTECHO587.1
764 Laney, S. R., Krishfield, R. A., Toole, J. M., Hammar, T. R., Ashjian, C. J., & Timmermans, M.-L. (2014).
765 Assessing algal biomass and bio-optical distributions in perennially ice-covered polar ocean ecosystems.
766 *Polar Science*, *8*(2), 73–85. https://doi.org/10.1016/j.polar.2013.12.003
767 Lawaetz, A. J., & Stedmon, C. A. (2009). Fluorescence intensity calibration using the Raman scatter peak of water.
768 *Applied Spectroscopy*, *63*(8), 936–940. https://doi.org/10.1366/000370209788964548.
769 Makarewicz, A., Kowalczuk, P., Sagan, S., Granskog, M. A., Pavlov, A. K., Zdun, A., et al. (2018). Characteristics
770 of chromophoric and fluorescent dissolved organic matter in the Nordic Seas. *Ocean Science*, *14*(3), 543–
771 562. https://doi.org/10.5194/os-14-543-2018
772 Mann, P. J., Spencer, R. G. M., Hernes, P. J., Six, J., Aiken, G. R., Tank, S. E., et al. (2016). Pan-Arctic Trends in
773 Terrestrial Dissolved Organic Matter from Optical Measurements. *Frontiers in Earth Science*, *4*.
774 https://doi.org/10.3389/feart.2016.00025
775 McLaughlin, F. A., Carmack, E. C., Macdonald, R. W., Melling, H., Swift, J. H., Wheeler, P. A., et al. (2004). The
776 joint roles of Pacific and Atlantic-origin waters in the Canada Basin, 1997–1998. *Deep Sea Research Part*
777 *I: Oceanographic Research Papers*, *51*(1), 107–128. https://doi.org/10.1016/j.dsr.2003.09.010
778 Morison, J., Kwok, R., Peralta-Ferriz, C., Alkire, M., Rigor, I., Andersen, R., & Steele, M. (2012). Changing Arctic
779 Ocean freshwater pathways. *Nature*, *481*(7379), 66–70. https://doi.org/10.1038/nature10705

780 Murphy, K. R., Butler, K. D., Spencer, R. G. M., Stedmon, C. A., Boehme, J. R., & Aiken, G. R. (2010).
781 Measurement of Dissolved Organic Matter Fluorescence in Aquatic Environments: An Interlaboratory
782 Comparison. *Environmental Science & Technology*, *44*(24), 9405–9412. https://doi.org/10.1021/es102362t
783 Osadchiev, A. A., Pisareva, M. N., Spivak, E. A., Shchuka, S. A., & Semiletov, I. P. (2020). Freshwater transport
784 between the Kara, Laptev, and East-Siberian seas. *Scientific Reports*, *10*(1), 13041.
785 https://doi.org/10.1038/s41598-020-70096-w
786 Overeem, I., & Syvitski, J. P. M. (2010). Shifting discharge peaks in arctic rivers, 1977–2007. *Geografiska Annaler:*
787 *Series A, Physical Geography*, *92*(2), 285–296. https://doi.org/10.1111/j.1468-0459.2010.00395.x
788 Peralta-Ferriz, C., & Woodgate, R. A. (2015). Seasonal and interannual variability of pan-Arctic surface mixed layer
789 properties from 1979 to 2012 from hydrographic data, and the dominance of stratification for multiyear
790 mixed layer depth shoaling. *Progress in Oceanography*, *134*, 19–53.
791 https://doi.org/10.1016/j.pocean.2014.12.005
792 Peterson, B. J., Holmes, R. M., McClelland, J. W., Vörösmarty, C. J., Lammers, R. B., Shiklomanov, A. I., et al.
793 (2002). Increasing River Discharge to the Arctic Ocean. *Science*, *298*(5601), 2171–2173.
794 https://doi.org/10.1126/science.1077445
795 Polyakov, I. V., Rippeth, T. P., Fer, I., Alkire, M. B., Baumann, T. M., Carmack, E. C., et al. (2020). Weakening of
796 Cold Halocline Layer Exposes Sea Ice to Oceanic Heat in the Eastern Arctic Ocean. *Journal of Climate*,
797 *33*(18), 8107–8123. https://doi.org/10.1175/JCLI-D-19-0976.1
798 Rabe, B., Schauer, U., Ober, S., Horn, M., Hoppmann, M., Korhonen, M., et al. (2016a). Physical oceanography
799 during POLARSTERN cruise PS94 (ARK-XXIX/3) [Data set]. *Alfred Wegener Institute, Helmholtz Centre*
800 *for Polar and Marine Research, Bremerhaven*. PANGAEA. https://doi.org/10.1594/PANGAEA.859558
801 Rabe, B., Schauer, U., Ober, S., Horn, M., Hoppmann, M., Korhonen, M., et al. (2016b, April 13). Physical
802 oceanography measured on water bottle samples during POLARSTERN cruise PS94 (ARK-XXIX/3).
803 *Alfred Wegener Institute, Helmholtz Centre for Polar and Marine Research, Bremerhaven*. PANGAEA.
804 https://doi.org/10.1594/PANGAEA.859559
805 Rudels, B., Anderson, L. G., & Jones, E. P. (1996). Formation and evolution of the surface mixed layer and
806 halocline of the Arctic Ocean. *Journal of Geophysical Research: Oceans*, *101*(C4), 8807–8821.
807 https://doi.org/10.1029/96JC00143

808 Rudels, B., Friedrich, H., & Quadfasel, D. (1999). The Arctic Circumpolar Boundary Current. *Deep Sea Research*
809 *Part II: Topical Studies in Oceanography*, *46*(6), 1023–1062. https://doi.org/10.1016/S0967-
810 0645(99)00015-6
811 Rudels, B., Muench, R. D., Gunn, J., Schauer, U., & Friedrich, H. J. (2000). Evolution of the Arctic Ocean boundary
812 current north of the Siberian shelves. *Journal of Marine Systems*, *25*(1), 77–99.
813 https://doi.org/10.1016/S0924-7963(00)00009-9
814 Rudels, B., Jones, E. P., Schauer, U., & Eriksson, P. (2004). Atlantic sources of the Arctic Ocean surface and
815 halocline waters. *Polar Research*, *32*(2), 181–208.
816 Serreze, M. C., Barrett, A. P., Slater, A. G., Woodgate, R. A., Aagaard, K., Lammers, R. B., et al. (2006). The large-
817 scale freshwater cycle of the Arctic. *Journal of Geophysical Research*, *111*(C11).
818 https://doi.org/10.1029/2005JC003424
819 Shimada, K. (2005). Halocline structure in the Canada Basin of the Arctic Ocean. *Geophysical Research Letters*,
820 *32*(3). https://doi.org/10.1029/2004GL021358
821 Stedmon, C. A., Thomas, D. N., Papadimitriou, S., Granskog, M. A., & Dieckmann, G. S. (2011b). Using
822 fluorescence to characterize dissolved organic matter in Antarctic sea ice brines. *Journal of Geophysical*
823 *Research*, *116*(G3). https://doi.org/10.1029/2011JG001716
824 Stedmon, C. A., Amon, R. M. W., Rinehart, A. J., & Walker, S. A. (2011a). The supply and characteristics of
825 colored dissolved organic matter (CDOM) in the Arctic Ocean: Pan Arctic trends and differences. *Marine*
826 *Chemistry*, *124*(1–4), 108–118. https://doi.org/10.1016/j.marchem.2010.12.007
827 Stedmon, C. A., & Cory, R. M. (2014). Biological origins and fate of fluorescent dissolved organic matter in aquatic
828 environments. *Aquatic Organic Matter Fluorescence*, 278–299.
829 https://doi.org/10.1017/CBO9781139045452.013
830 Stedmon, C. A., & Nelson, N. B. (2015). The Optical Properties of DOM in the Ocean. In *Biogeochemistry of*
831 *Marine Dissolved Organic Matter* (pp. 481–508). Elsevier. https://doi.org/10.1016/B978-0-12-405940-
832 5.00010-8
833 Steele, M., & Boyd, T. (1998). Retreat of the cold halocline layer in the Arctic Ocean. *Journal of Geophysical*
834 *Research: Oceans*, *103*(C5), 10419–10435. https://doi.org/10.1029/98JC00580

Steele, M., Morison, J., Ermold, W., Rigor, I., Ortmeyer, M., & Shimada, K. (2004). Circulation of summer Pacific halocline water in the Arctic Ocean. *Journal of Geophysical Research: Oceans*, *109*(C2). https://doi.org/10.1029/2003JC002009

Timmermans, M.-L., Toole, J., & Krishfield, R. (2018). Warming of the interior Arctic Ocean linked to sea ice losses at the basin margins. *Science Advances*, *4*(8), eaat6773. https://doi.org/10.1126/sciadv.aat6773

Toole, J., Krishfield, R., Timmermans, M.-L., & Proshutinsky, A. (2011). The Ice-Tethered Profiler: Argo of the Arctic. *Oceanography*, *24*(3), 126–135. https://doi.org/10.5670/oceanog.2011.64

Toole, J. M., Timmermans, M.-L., Perovich, D. K., Krishfield, R. A., Proshutinsky, A., & Richter-Menge, J. A. (2010). Influences of the ocean surface mixed layer and thermohaline stratification on Arctic Sea ice in the central Canada Basin. *Journal of Geophysical Research: Oceans*, *115*(C10). https://doi.org/10.1029/2009JC005660

Toole, J. M., Krishfield, R., & Woods Hole Oceanographic Institution Ice-Tethered Profiler Program. (2016). Ice-Tethered Profiler observations: Vertical profiles of temperature, salinity, oxygen, and ocean velocity from an Ice-Tethered Profiler buoy system [Data set]. NOAA National Centers for Environmental Information. https://doi.org/10.7289/V5MW2F7X

Walker, S. A., Amon, R. M. W., & Stedmon, C. A. (2013). Variations in high-latitude riverine fluorescent dissolved organic matter: A comparison of large Arctic rivers. *Journal of Geophysical Research: Biogeosciences*, *118*(4), 1689–1702. https://doi.org/10.1002/2013JG002320

Williford, T., Amon, R. M. W., Benner, R., Kaiser, K., Bauch, D., Stedmon, C., et al. (2021). Insights into the origins, molecular characteristics and distribution of iron-binding ligands in the Arctic Ocean. *Marine Chemistry*, *231*, 103936. https://doi.org/10.1016/j.marchem.2021.103936

Woodgate, R. A., Aagaard, K., Swift, J. H., Smethie, W. M., & Falkner, K. K. (2007). Atlantic water circulation over the Mendeleev Ridge and Chukchi Borderland from thermohaline intrusions and water mass properties. *Journal of Geophysical Research: Oceans*, *112*(C2). https://doi.org/10.1029/2005JC003416

Yamashita, Y., & Tanoue, E. (2008). Production of bio-refractory fluorescent dissolved organic matter in the ocean interior. *Nature Geoscience*, *1*(9), 579–582. https://doi.org/10.1038/ngeo279

Zabłocka, M., Kowalczuk, P., Meler, J., Peeken, I., Dragańska-Deja, K., & Winogradow, A. (2020). Compositional differences of fluorescent dissolved organic matter in Arctic Ocean spring sea ice and surface waters north of Svalbard. *Marine Chemistry*, *227*, 103893. https://doi.org/10.1016/j.marchem.2020.103893

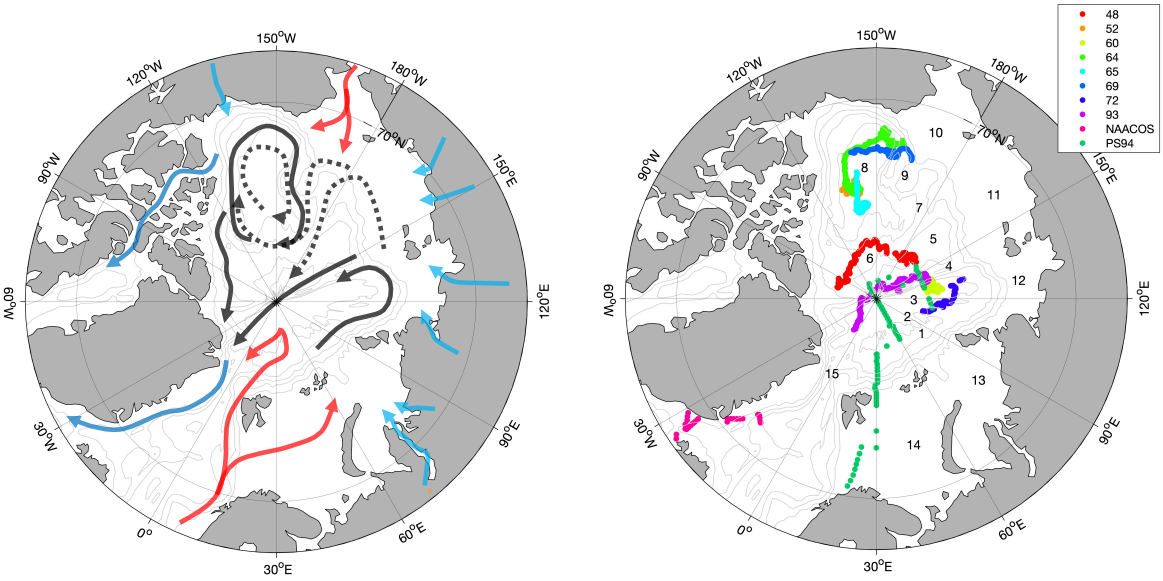

Figure 1. Left: schematic of general circulation pathways. Red arrows indicate inflowing ocean water; blue arrows polar water exiting the Arctic, light blue are major Arctic rivers. Black arrows indicate the two major circulation patterns of the central Arctic, Transpolar Drift extending from the Siberian shelf over the North Pole towards the Fram Strait, and the Beaufort Gyre. Solid and dotted lines indicate the position of these features during a positive and negative Arctic Oscillation (Morison et al 2012). Right: ITP drift pathways, and cruise stations. The legend indicates the ITP and cruise identity. The numbers on the map indicate geographic areas as follows: 1) Nansen Basin; 2) Gakkel Ridge; 3) Amundsen Basin; 4) Lomonosov Ridge; 5) Makarov Basin; 6) Alpha Ridge; 7) Mendeleev Ridge; 8) Beaufort Gyre; 9) Chukchi Plateau; 10)

875 Chukchi Sea; 11) East Siberian Sea; 12) Laptev Sea; 13) Kara Sea; 14) Barents Sea; 15) Fram
876 Strait.

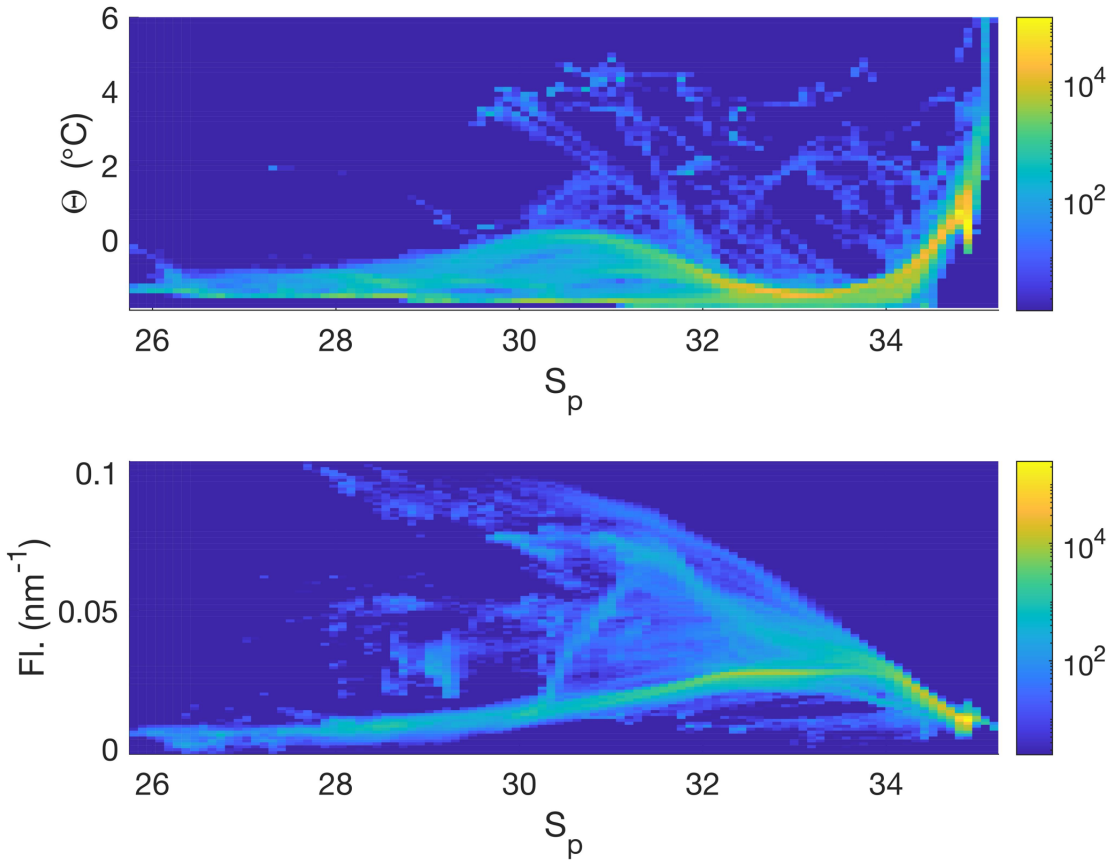

877

878 **Figure 2**. 2D histograms of potential temperature (top panel) and DOM fluorescence (bottom
879 panel) against practical salinity for all observations included in the study (0-800 m). Note that
880 data with temperatures warmer than 6 ºC are not shown.

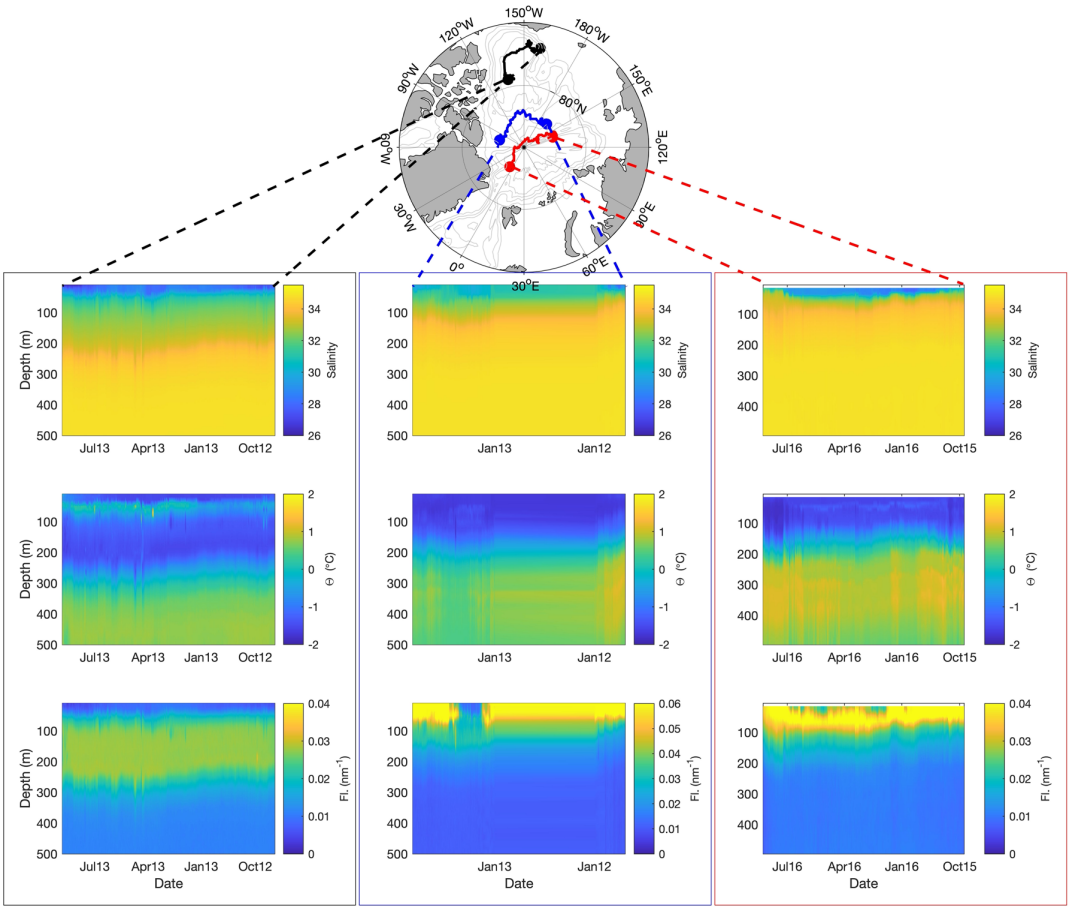

881

882 **Figure 3.** Section plots along the trajectories of ITP 64 (left column), 48 (middle column) and 93
883 (right column) for salinity (top row), potential temperature (middle row) and DOM fluorescence
884 (bottom row). The links to the map indicate where trajectories start and end. Note that the DOM

885 fluorescence scale is varies and that there are data from ITP 48 and 93 that are off scale (above
886 the maximum shown).

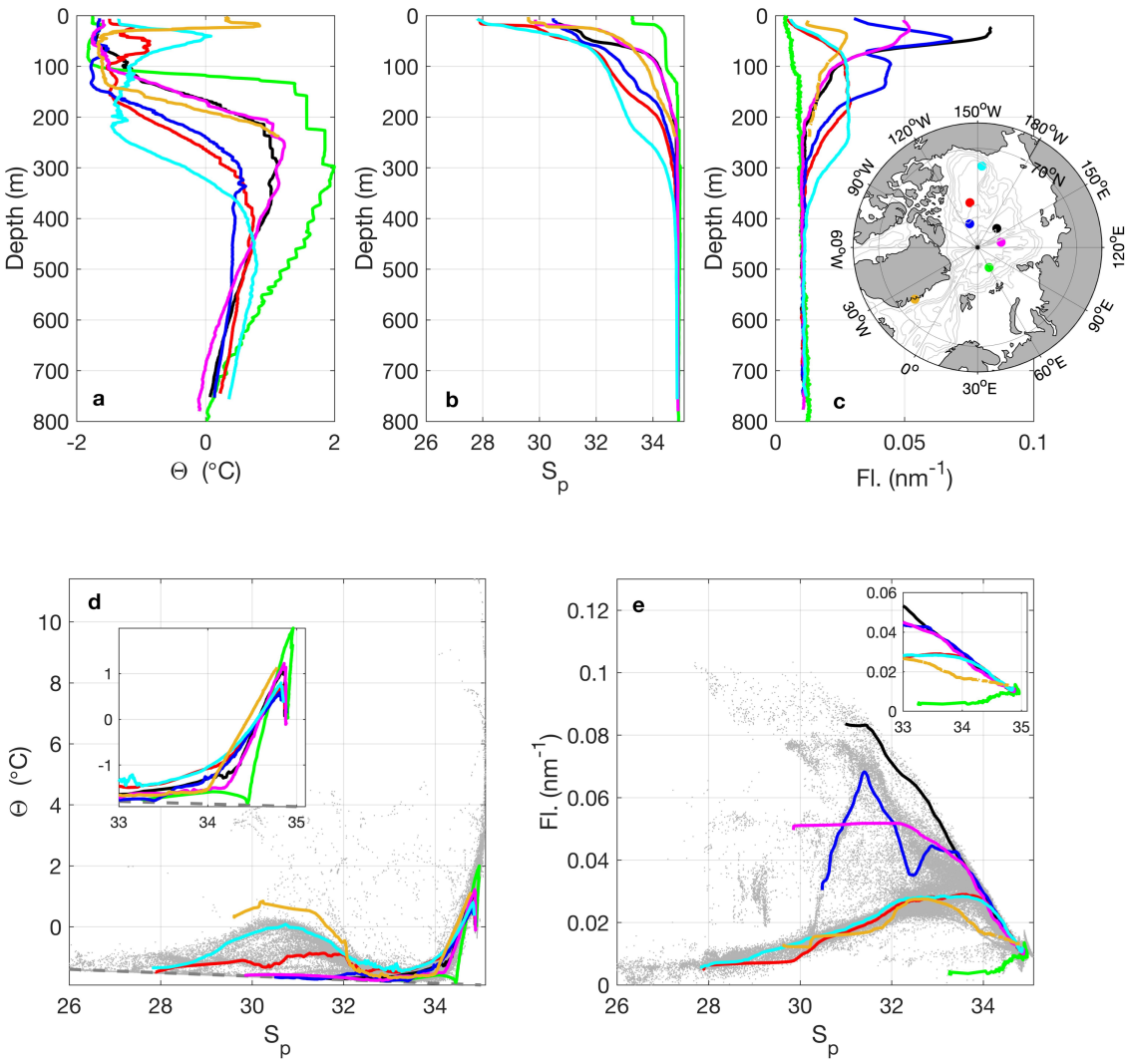

887

888 **Figure 4.** Archetypical water column profiles of a) potential temperature, b) practical salinity
889 and c) DOM fluorescence. The lower panels show property-property plots of d) potential
890 temperature against practical salinity (freezing temperature as grey dashed line) and e) DOM

fluorescence against salinity. Green-PS94; Magenta-ITP60; Black-ITP48; Blue-ITP48; Red-ITP65; Cyan-ITP64; Brown-NAACOS.

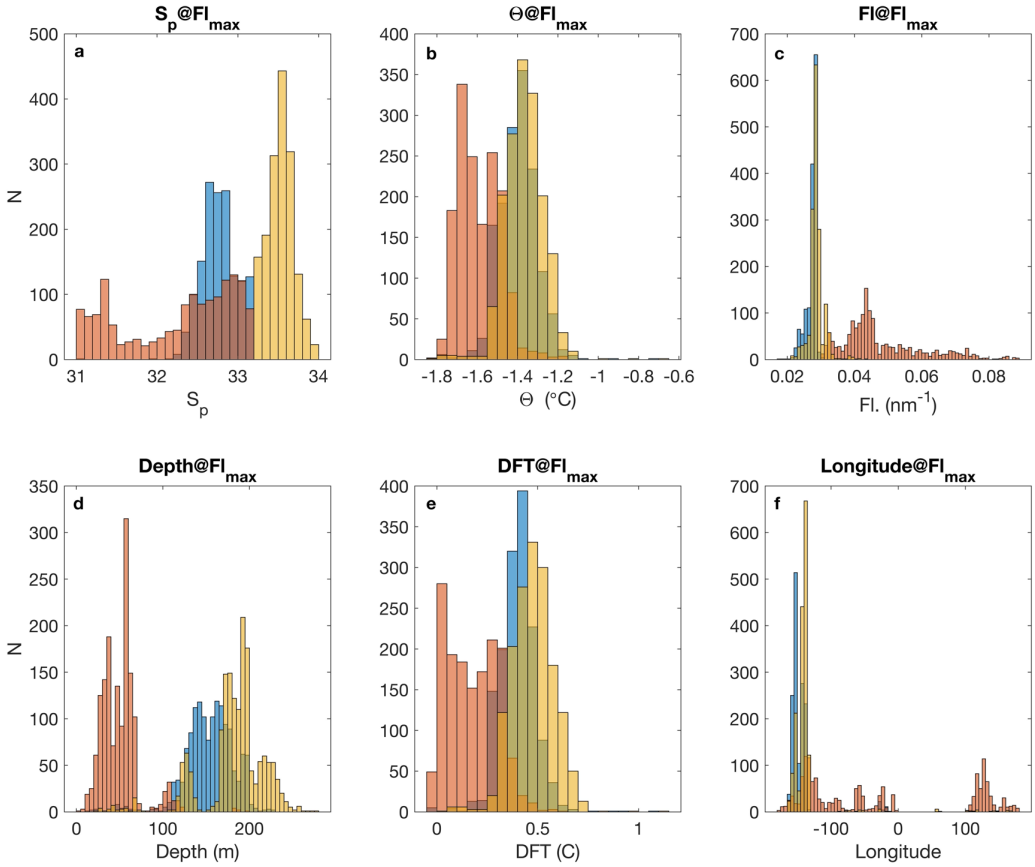

Figure 5. Histograms of properties of the DOM fluorescence maximum in the halocline (S 31-34). The data are colored with respect to three groups, to illustrate different features: blue-salinity 31-33.2 and DOM fluorescence <0.0305 nm^{-1}; red-salinity 31-33.2 and DOM fluorescence >0.0305 nm^{-1}; yellow-salinity>33.2; a) practical salinity; b) potential temperature; c) DOM fluorescence; d) depth of DOM fluorescence maximum; e) deviation from freezing

899 temperature; and f) distribution of longitudinal position (positive is east of meridian) between
900 groups.

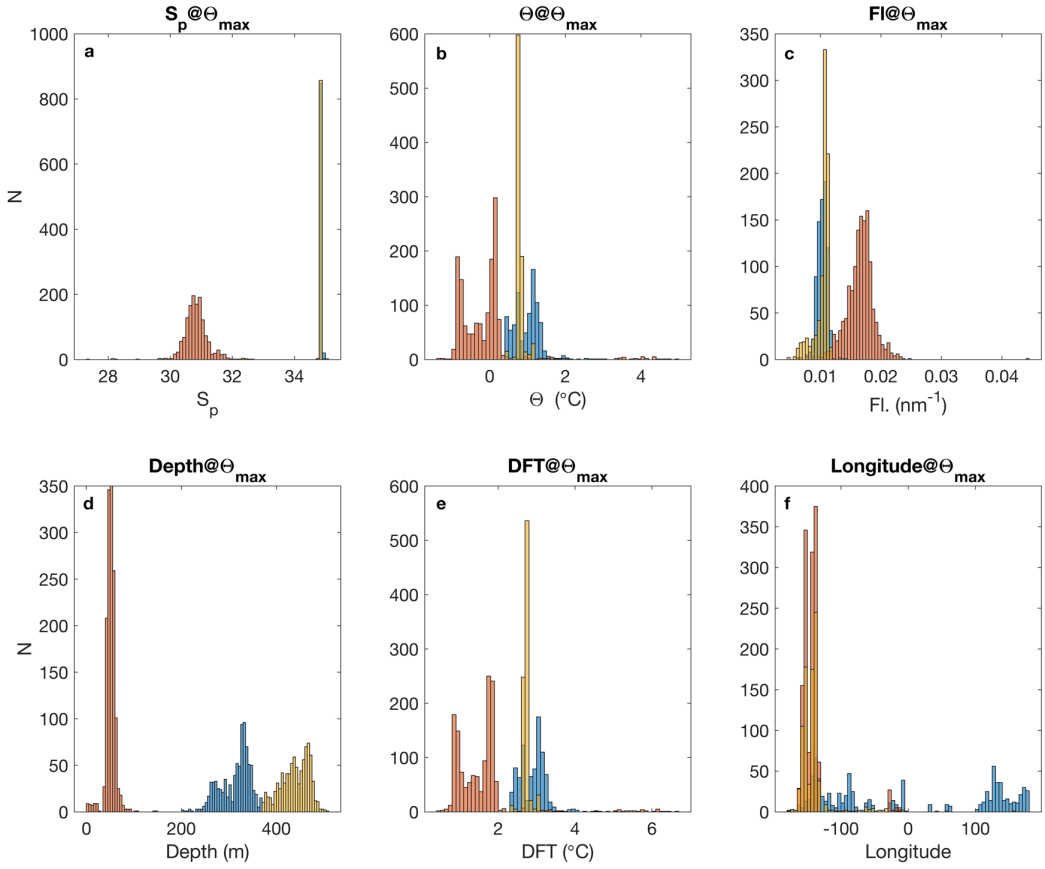

901

902 **Figure 6.** Histograms of properties of the potential temperature maximum. The data are colored
903 to illustrate different features: blue-salinity >33 and depth between 200 and 370 m; red-
904 salinity<33; yellow-salinity>33; a) practical salinity; b) potential temperature; c) DOM

fluorescence; d) depth of temperature maximum; e) deviation from freezing temperature; and f) distribution of longitudinal position (positive is east of meridian) between groups.

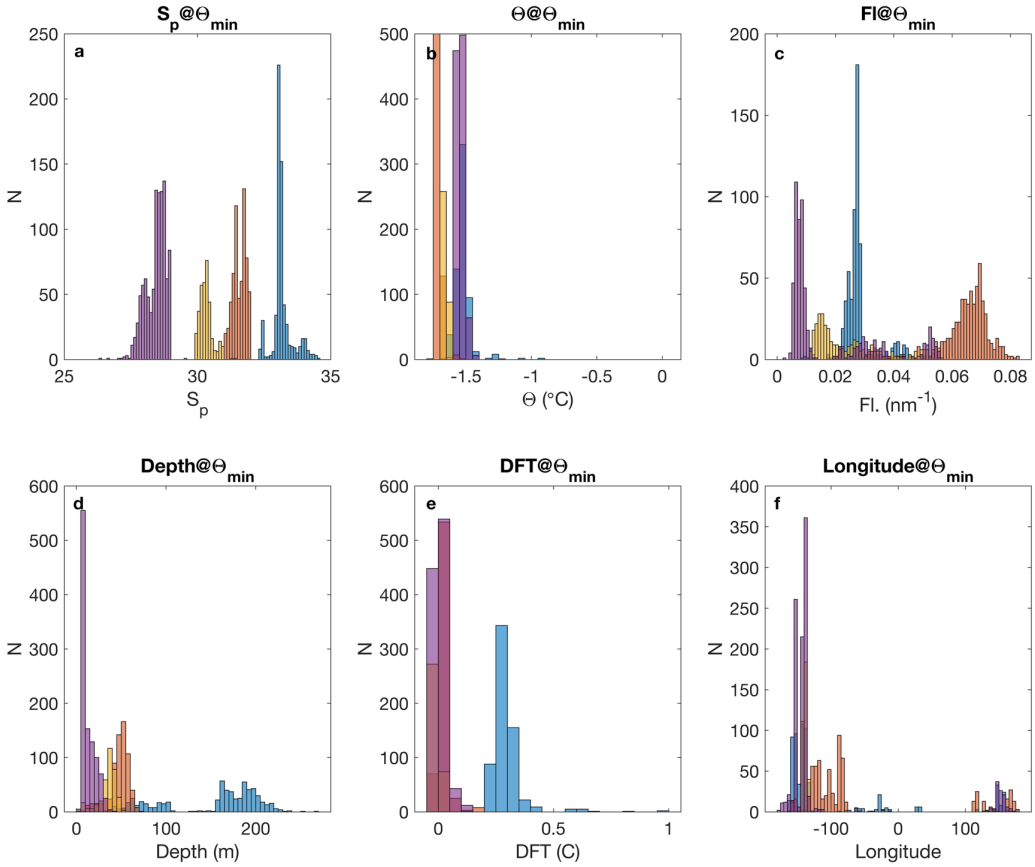

Figure 7. Histograms of properties of the potential temperature minimum. The data are colored to illustrate different features: blue - deviation from freezing temperature > 0.2 ºC; red - deviation from freezing temperature < 0.2 ºC and 31<S<32; yellow - deviation from freezing temperature < 0.2 ºC and 29.5<S<31; purple - deviation from freezing temperature < 0.2 ºC and salinity <29; a) practical salinity; b) potential temperature; c) DOM fluorescence; d) depth of

913 temperature minimum; e) deviation from freezing temperature; and f) distribution of longitudinal
914 position (positive is east of meridian) between groups.

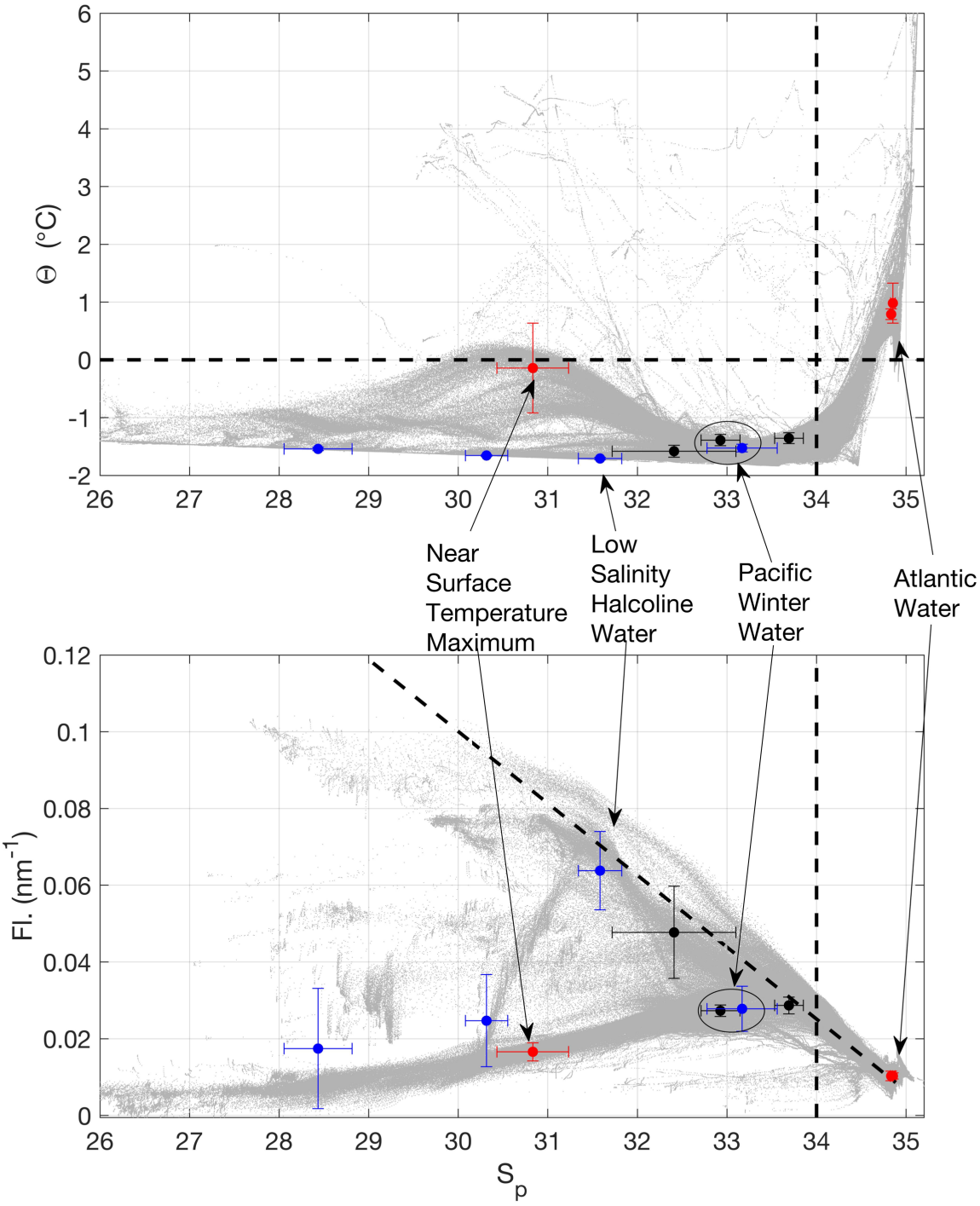

915

916 **Figure 8.** Mean endmembers characteristics from the analysis of temperature maximum (red),
917 temperature minimum (blue) and DOM fluorescence (black) maximum properties plotted
918 together will all data (grey). The error bars indicate standard deviation. The top graph is potential
919 temperature against practical salinity and the bottom graph is DOM fluorescence against
920 practical salinity. The horizontal dashed line represents the 0 ºC isotherm and the vertical line the
921 34 isohaline. The diagonal represents a theoretical mixing line between Siberian shelf water
922 (Gonçalves-Araujo et al., 2016) and Atlantic water.

923

924 **Table 1.** Summary of the available data after quality control of the profile data. Only profiles
925 with complete records of temperature, salinity and CDOM fluorescence were selected.

Platform	Fluorescence Sensor***	Start (ITP deployment region)	End	# Profiles	Source
ITP48	*ECO* FLbb-CD	10/Sep/2011 (Lomonosov Ridge)	29/Oct/2012	1302	(Laney et al., 2014; Toole et al., 2016)
ITP52	*ECO* FLbb-CD	6/Aug/2011 (Beaufort Gyre)	14/Nov/2011	363	(Laney et al., 2014; Toole et al., 2016)
ITP60	*ECO* FLbb-CD	15/Sep/2012 (Amundsen Basin)	23/Dec/2012	259	(Laney et al., 2014; Toole et al., 2016)
ITP64	*ECO* FLbb-CD	29/Aug2012 (Beaufort Gyre)	25/Aug/2013	1079	(Laney et al., 2014; Toole et al., 2016)
ITP65	*ECO* FLbb-CD	28/Aug/2012 (Beaufort Gyre)	18/Feb/2013	397	(Toole et al., 2016)
ITP69	*ECO* FLbb-CD	29/Aug/2013 (Chukchi Plateau)	15/Feb/2014	343	(Toole et al., 2016)
ITP72	*ECO* FLbb-CD	31/Aug/2013 (Amundsen Basin)	16/Dec/2013	216	(Toole et al., 2016)
ITP93	*ECO* FLbb-CD	24/Sep/2015 (Lomonosov Ridge)	8/Aug/2016	944*	(Rabe et al., 2016a, 2016b)
PS94	DrHaardt	18/Aug/2015	9/Oct/2015	81**	(Rabe et al., 2016a, 2016b)
NAACOS	WETStar	3/Sep/2012	12/Sep/2012	60	unpublished

926 *Profiles after profile 955 are not included due to failure of the conductivity sensor.
927 ** Data from depths greater than 800m (max depth covered by ITPs) are not included in the
928 analysis.

929 ***ECO FLbb-CD and WETStar (both WET Labs Inc.): Excitation 370 and emission 460 nm;
930 DrHaardt: Excitation 350 – 460 nm, emission 550 nm.